Laponite and hybrid surfactant/laponite particles processed as spheres by spray-drying†

Laurent Bippus, Maguy Jaber and Bénédicte Lebeau*

Received (in Montpellier, France) 14th November 2008, Accepted 28th January 2009
First published as an Advance Article on the web 6th March 2009
DOI: 10.1039/b820429b

Laponite elementary disc crystals dispersed in water in the presence or absence of non-ionic Brij58 surfactant have been used as nanobuilding blocks to form laponite and laponite/surfactant spherical particles by spray-drying. The size distribution of the spherical spray-dried particles ranges from 70 to 1000 nm (average size about 220 nm). Although raw laponite (RL) was almost totally exfoliated in water, the spray-dried spherical particles were found partially delaminated and stable when spread into water. Based on a full characterization by several techniques such as dynamic light scattering, scanning and transmission electron microscopies, X-ray diffraction, thermal analyses, nitrogen volumetric sorption and solid-state multi-nuclear NMR studies, a mechanism has been proposed to explain the formation of the spherical micron size particles: a face-to-face and edge-to-edge stacking of the elementary disc crystals leads to the formation of few-layer laponite platelets that aggregate within the restricted volume of water droplets during the drying stage. In the presence of Brij58, elementary disc crystals are covered by surfactant molecules adsorbed on their surface. As a consequence, surfactant molecules fill the interlayer space to form spherical Brij58/laponite nanocomposite particles. These spray-dried laponite and Brij58/laponite spherical particles present a high potential for sorption applications.

Introduction

During recent decades the interest towards nanoparticles has mainly increased because of their properties such as surface reactivity that are different from those of the bulk material. However, decreasing the size brings disadvantages such as toxicity[1] and/or manipulation difficulties.[2] Nanoparticles are interesting, not only for their unique properties, but also for their potential to be used as nanobuilding blocks. Interest in nanobuilding blocks is growing as they have been recognized to be basic units for the elaboration of hierarchically-organized materials by self-assembling processes.[3,4] As there are various types of inorganic nanobuilding blocks and several ways to link them together, the resulting materials are numerous.[5] Moreover, this strategy allows a better control of the structure of the final material and offers an easier shape modelling.

Materials resulting from nanobuilding blocks can be used in different application domains such as catalysts,[6,7] varnishes and adhesives;[8] or marginally in two-terminal circuit device nano-applications[9,10] or non-volatile random access memory.[11] Most nanobuilding units are nanocrystals that can be classified according to their one-, two- or three-dimensionalities[12] such as tubes, wires, plates,[13–15] multipods, crosses, stars.[16] These different dimensionalities lead to materials with various morphologies such as films,[17] fibres,[18,19] mushroom-like particles,[20] spheres,[21,22] or monoliths.[23]

In order to control the self-assembly process of nanoobjects for the elaboration of hierarchically organized materials, several techniques have been identified, for instance gas-phase synthesis,[24] emulsion-based methods,[25] templated approach[26] or spray-drying.[27] The latter is a technique which is being increasingly used because of its distinctive ability to easily control morphology by leading to spherical particles, moreover, it could be developed at the industrial level.

The aerosol process has already been used to synthesize many materials. Coupling with an evaporation-induced self-assembly (EISA) mechanism,[28,29] it has been particularly studied to form silica–surfactant mesostructures such as spherical mesoporous particles[28–33] and hollow spheres,[34] nanocrystalline transition-metal oxide spheres[35] and spherical organotalc particles.[36] Colloidal suspensions of pre-formed objects such as silica nanoparticles were also used as precursor solutions to form spherical mesostructured materials.[37] One interest of the aerosol process is to confine the reaction volume inside spherical solvent droplets.

We have proceeded to the elaboration of spherical laponite particles from the spray-drying of colloidal laponite suspensions stabilized with a non-ionic surfactant or in its absence. Laponite is a synthetic industrial clay of the smectite family, and is known as a 2 : 1 phyllosilicate whose primary nanoparticles—constituted of aggregates of stacked elementary discs particles—are about 100 nm.[38] Laponite is known to delaminate when spread out into water in a 10 min process at room temperature and to form colloidal suspensions.[39] Moreover, it has been

Equipe Matériaux à Porosité Contrôlée, Institut de Sciences des Matériaux de Mulhouse, LRC CNRS 7228, Université de Haute-Alsace, ENSCMu, 3 rue Alfred Werner, 68093, Mulhouse cedex, France. E-mail: benedicte.lebeau@univ-mulhouse.fr; Fax: +33389336885; Tel: 33389336882

† Electronic supplementary information (ESI) available: Fig. SM1: Thermogravimetric curves of surfactant-free materials and Brij58/laponite materials. Fig. SM2: FTIR spectra of (a) RL, (b) SDL and (c) SDL/B-4 samples. Fig. SM3: ^{29}Si MAS-DEC NMR spectra RL and SDL samples. Fig. SM4: ^{1}H MAS-NMR spectra of dehydrated RL and SDL samples. See DOI: 10.1039/b820429b

proved that laponite forms structured gels in concentrated dispersions.[40] Due to these properties, laponite is mainly used in industry as a rheological modifier and film former. However, laponite and surface modified laponite have also been used for adsorption of dyes[41,42] surfactants[43] and biomolecules.[44]

In the present study, laponite elementary disc crystals and laponite stacked discs resulting from the exfoliation of raw laponite and forming a colloidal suspension have been used as nanobuilding blocks. A non-ionic surfactant has also been added to the colloidal laponite suspension in order to stabilize it and to elaborate surfactant/laponite nanocomposites. Indeed, Mongondry *et al.* have showed that laponite colloidal suspensions can be stabilized with a Brij-type surfactant by steric protection of the polymeric chains.[45] Brij58 was selected as it was reported to be the best stabilizer agent for laponite.[46]

Samples were characterized by dynamic light scattering (DLS), scanning electron microscopy (SEM), transmission electron microscopy (TEM), X-ray diffraction (XRD), thermogravimetric/thermodifferential analyses (TGA/TDA), nitrogen sorption, Fourier-transform infrared (FTIR) and ^{1}H, ^{7}Li, ^{29}Si and ^{13}C NMR spectroscopies. From these structural and textural analyses a mechanism of formation of the resulting spherical laponite microparticles has been proposed.

The notation used for samples is as follows: RL = raw laponite, SDL = spray-dried laponite, = SDL/B-*x* = spray-dried Brij58/laponite nanocomposite (*x* indicates the initial concentration of Brij58), 473K-DL = 473 K-dried laponite.

Results and discussion

Precursor clay suspensions

The as-made 20 g L^{-1} laponite and Brij58/laponite colloidal suspensions were analyzed by DLS and size distributions are given in Fig. 1. The size distribution *vs.* scattered intensity of the laponite suspension showed a polydisperse distribution with three distinct populations of 3–10, 10–100 and 90–400 nm centred at about 8, 28 and 160 nm, respectively (Fig. 1(b)). However, DLS size measurements *vs.* number of particles showed only one population ranging from 3 to 10 nm and centred at 5–6 nm indicating that this population is in the majority (Fig. 1(a)). Considering the size range it unambiguously corresponds to elementary crystal discs and stacked elementary disc crystals (Fig. 2) although it is much smaller than the expected value at 25 nm[38,47–49] Size distribution scales given by the DLS technique are most probably erroneous because of the shape of the particles which is very far from the ideal case of spheres. However, DLS results can be considered for the observed tendencies and thus for following the size distribution variations. The two minority populations at 28 and 160 nm could be attributed to aggregated stacked elementary disc particles (primary particles) and clusters of aggregated stacked elementary disc particles (Fig. 2) whose size diameter was previously reported to be at 35 and 100 nm, respectively.[39,50] The presence of mainly elementary crystal discs in the suspension reflects a quasi total exfoliation of the initial laponite particles.[39]

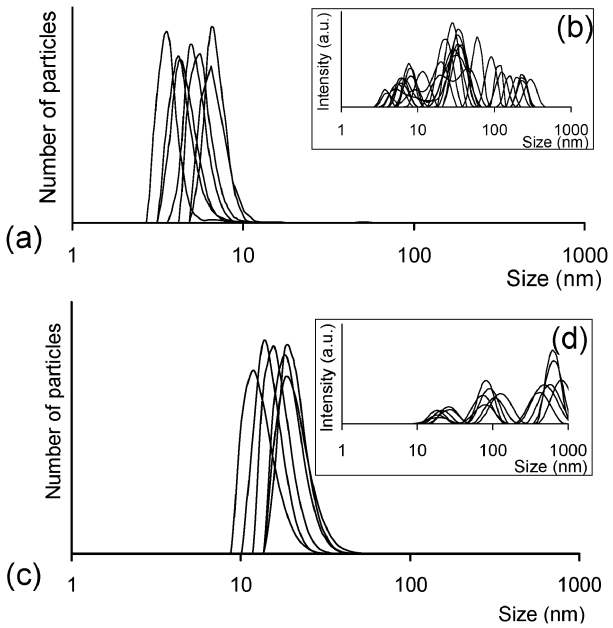

Fig. 1 DLS size distribution of (a), (b) raw laponite™ and (c), (d) Brij™/laponite™ composite in mother-liquors for spray-drying. Insets are distributions *vs.* intensity.

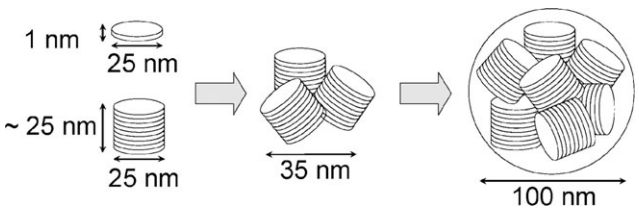

Fig. 2 Schematic representation of laponite particles: (a) elementary disc crystals and stacked discs; (b) aggregate of stacked discs;[55] (c) cluster of stacked discs.[39]

A major size population from 10 to 30 nm was observed for Brij58/laponite suspensions indicating the main presence of aggregated stacked elementary disc particles (Fig. 1(c)). The stacking of elementary disc crystals and the subsequent aggregation are probably due to the presence of Brij58 surfactant molecules on the surfaces and edges of elementary disc surfaces[51,52] that interact between themselves (Fig. 3). From the laponite unit cell and laponite nanodisc dimensions, the number of unit cell per nanodisc was estimated to be around 1000. For 2, 4, 6 and 8 g L^{-1} concentrations of Brij58, the

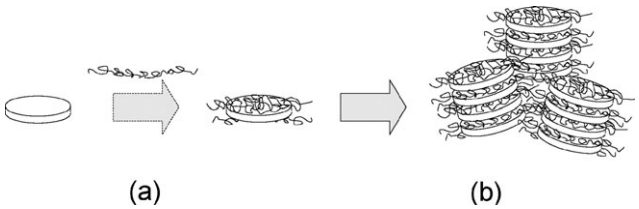

Fig. 3 Schematic representation of (a) Brij58 surfactant adsorption onto a laponite elementary disc crystal[56] and (b) stacking of Brij58/laponite elementary disc crystals

number of CH_2CH_2O groups per accessible siloxane site (8 per unit cell) is, respectively, 0.16, 0.31, 0.47 and 0.63. These values seem to indicate that the laponite nanodisc surfaces are not saturated for the adsorption of Brij58 molecules, which it is in agreement with the observations of Mongondry *et al.*[45]

Similarly to the raw laponite suspension, three populations were observed for Brij58/laponite suspensions on the scattered intensity DLS diagram (Fig. 1(d)) but the two at 100 and 600 nm are in minority. It is noteworthy that sizes characteristic of populations observed by DLS are one decade greater for Brij58/laponite suspensions which reflects a higher degree of aggregation in the presence of surfactant.

Elaboration of spray-dried clay particles

For all spray-dried laponite and Brij58/laponite samples, powders less dense than the raw laponite clay were obtained. The apparent volumic mass of raw laponite measured by simply weighing and measuring the volume occupied by the clay powder in a vial is about 1000 kg m^{-3} *cf.* 500 kg m^{-3} for the spray-dried laponite and 600 kg m^{-3} for the spray-dried Brij58/laponite nanocomposites.

Spray-dried laponite and Brij58/laponite powders were spread out into water at 5 g L^{-1} concentration for DLS analyses. The DLS size distributions *vs.* the number of the particles are reported on Fig. 4. The size distribution *vs.* the number of particles obtained from DLS, exhibit one broad band indicating the presence of a majority population ranging from 100 to 300 nm and centred at 200 nm. Two other populations from 200 to 1000 nm and 600 to 2000 nm and centred at 500 and 1000 nm, respectively, were also present as clearly observed on the curves of size *vs.* intensity. Similar size distributions were observed for SDL/B-*x* particles. These

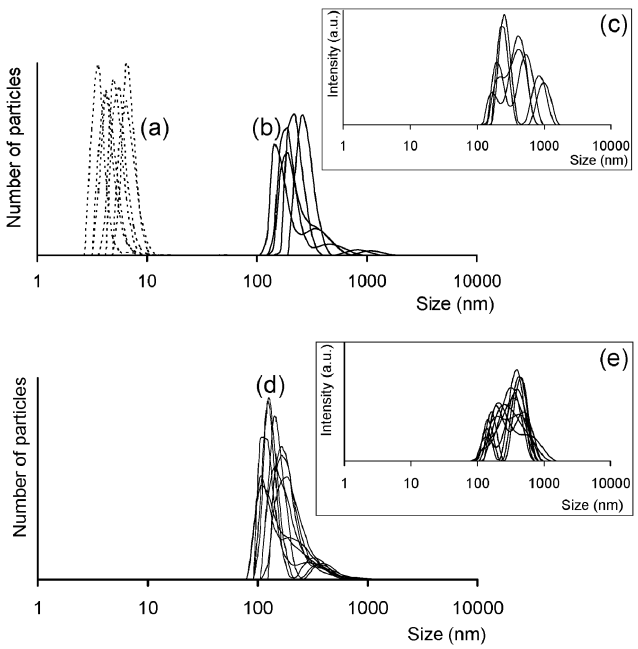

Fig. 4 DLS size distribution of (a) raw laponite™ (dotted lines); (b) and (c) of sprayed laponite™; (d) and (e) of laponite™/Brij™ composite SDL/B-8. Insets are size distributions *vs.* intensity.

results indicate the formation of larger particles under spray-drying process.

Samples were then observed by SEM and representative micrographs of RL, 473K-DL and SDL samples are reported in Fig. 5. Low magnification SEM micrographs show that RL and 473K-DL are composed of large aggregates, which appear with irregular shape for RL but seem to have a plate-like morphology for the 473K-DL sample. The SDL sample presents a powdery aspect at this macroscopic scale. High magnification shows roughness for both RL and 473K-DL samples while spherical objects are clearly observed for the SDL sample. At higher magnification, 30 nm-diameter spherical particles can be distinguished in RL and 473K-DL samples. These nanoparticles most probably correspond to aggregates of stacked elementary discs and seem to be more packed in the 473K-DL sample probably as a result of the drying process at 200 °C.

For SDL and SDL/B-*x* samples, sphere-like particles were observed with mean diameter ranging from 70 nm to 1 μm reflecting a large particle size polydispersity. The SEM micrographs clearly account for the lower density of SDL and SDL/B-*x* samples compared to RL and 473K-DL samples. Furthermore, a certain roughness is observed at the surface of the spherical spray-dried particles: this may indicate the assembling of laponite stacked sheets in spherical confined volume.

Spheres were counted and their diameters were measured on representative SEM micrographs of SDL and SDL/B-*x* materials in order to determine their size distribution. Plots of diameter *vs.* number of particles are presented in Fig. 6. For all samples the size distribution was broad, ranging from 50 to 550 nm and roughly centred at 200 nm. These results are in good agreement with the size distribution obtained from DLS analysis and represented by the dotted line. It is noteworthy that the fact that spray-dried particles could be observed by DLS reflects their stability in water. This was confirmed by spreading out SDL into water at a ~1 g L^{-1} concentration for several days (up to 7) and then directly air-drying the suspension on the SEM support. Resulting SEM micrographs are similar to those taken from the initial SDL sample. The stability of 7-day aged spray-dried particles in water was also confirmed by DLS.

Samples were spread out in water (about 1 g L^{-1}) and air-dried onto copper grids for TEM analyses. Representative micrographs of RL, SDL and SDL/B-2 samples are reported in Fig. 7. RL exhibits particles (size about 100 nm) with undefined shape and more or less aggregated (Fig. 7(a)). At higher magnification, long-range stacked layers were observed with an interlayer distance measured from the micrograph of 1.44 nm (Fig. 7(b)). These TEM observations show that during the drying step, edge-to-edge and face-to-face stacking of laponite that was delaminated in water have occurred.

TEM observations (Fig. 7) confirm both the spherical morphology and the size polydispersity of the SDL and SDL/B-*x* samples that have been observed by SEM. However, TEM shows that spherical spray-dried particles are constituted by stacked ~100-nm length and ~30-nm height clay layers which are aggregated. This explains the roughness of the surface observed by SEM. Furthermore, TEM also

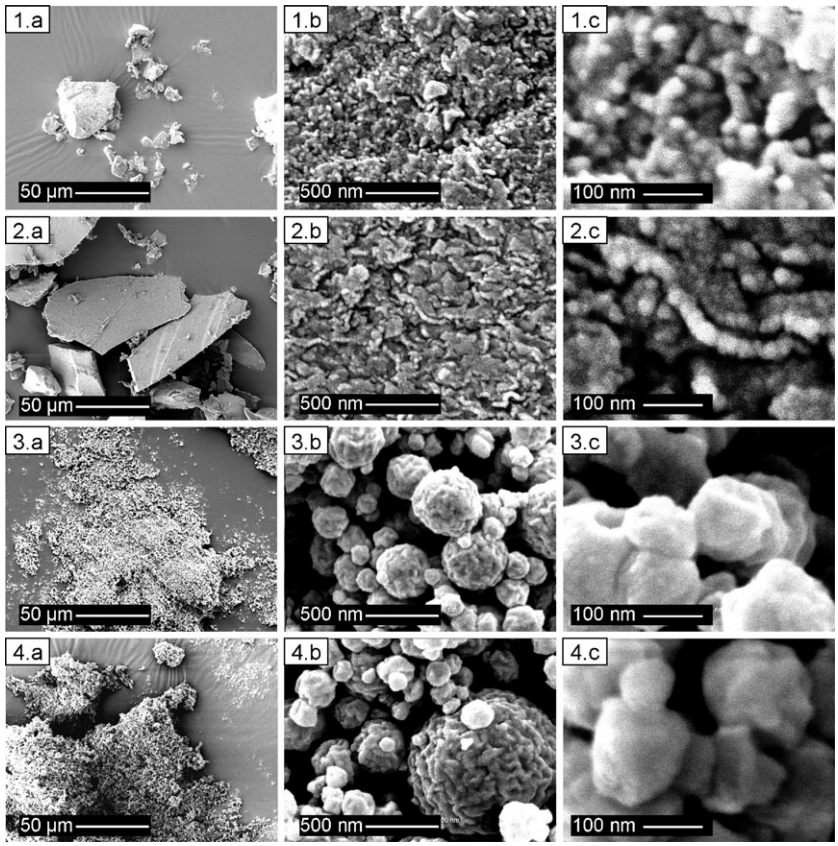

Fig. 5 Scanning electron micrographs of (1) raw laponite™, (2) 473 K-dried laponite™, (3) sprayed laponite™, and (4) laponite™/Brij™ composite SDL/B-8 at several magnifications ((a) ×500, (b) ×50 000 and (c) ×200 000).

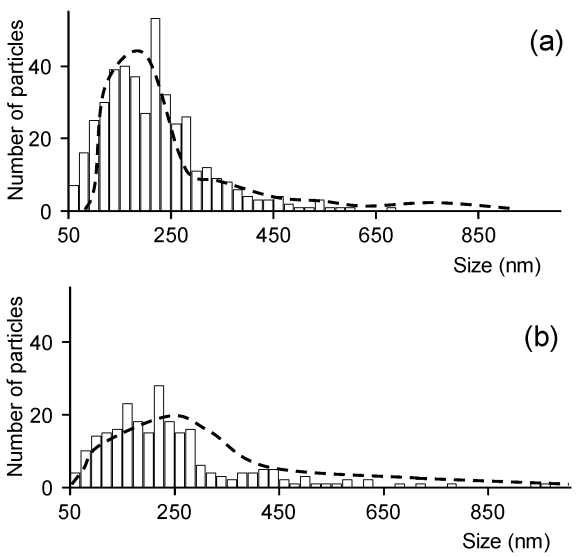

Fig. 6 Particle size distribution of (a) sprayed laponite™ and (b) laponite™/Brij™ composite SDL/B-8 determined by counting from SEM micrographs. The dotted lines represent size distributions determined by DLS.

shows a partial delamination of clay layers (see zoom in Fig. 7(b)).

The XRD patterns of the RL, 473 K-DL and SDL samples are displayed in Fig. 8A. All XRD patterns show broad diffraction peaks characteristic of the laponite clay structure.[53] The $d_{(060)}$ value (0.152 nm) is the same for all samples and its position confirms the trioctahedral character of the clays. Main differences are observed for the $d_{(001)}$ reflection. The theoretical thickness of the T:O:T layer is 0.96 nm. The structural unit, composed of the layer thickness and the interlayer space, is given by the *d*-value corresponding to the (001) basal reflection ($d_{(001)}$). This value is 1.37 nm in the laponite, which is in quite good agreement with TEM measurement (1.44 nm). The $d_{(001)}$ values are lower for 473 K-DL (1.29 nm) and SDL (1.05 nm) materials, indicating that there is less water in the interlayer space.

While a quasi-total delamination of the raw laponite was observed by DLS, the XRD show that elementary disc crystals have stacked during the drying processes at 473 K or by aerosol spraying. The SDL/B-*x* nanocomposite samples were also analyzed by XRD. For all compositions, patterns exhibit diffraction peaks indicating a laponite-like structure. However strong differences are observed in the $d_{(001)}$ region (Fig. 8(b)). The $d_{(001)}$ values are much higher in the presence of Brij58 and increase with the amount of surfactant (Fig. 8B). This indicates the presence of surfactant in the interlayer space. The increase of the $d_{(001)}$ value with the amount of Brij58 can be correlated to the increase of Brij58 amount in the interlayer space leading to different aggregation state of surfactant polymer chains.

Similarly to surfactant-free systems, DLS showed that laponite was quasi-totally exfoliated in water and the

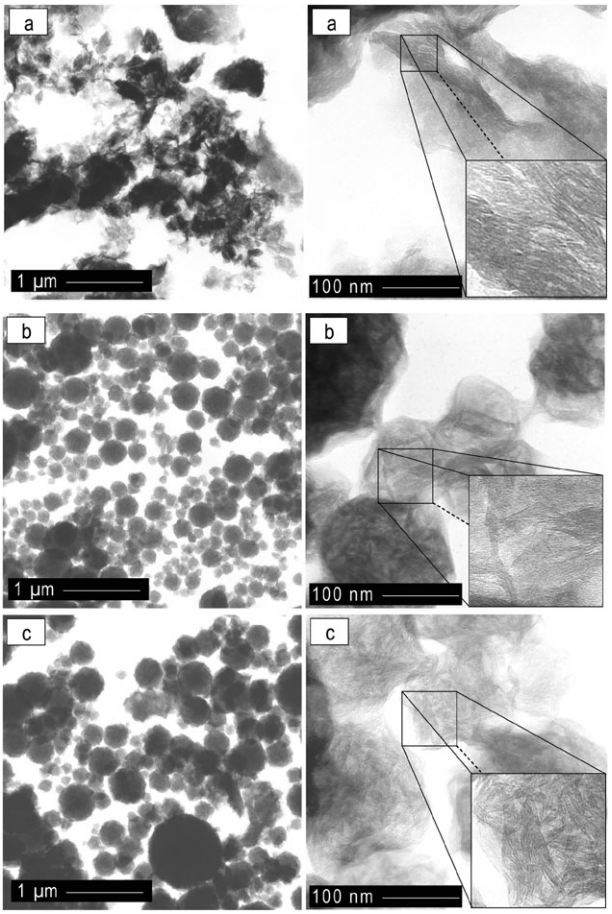

Fig. 7 TEM micrographs of (a) RL, (b) SDL and (c) SDL/B-2 samples

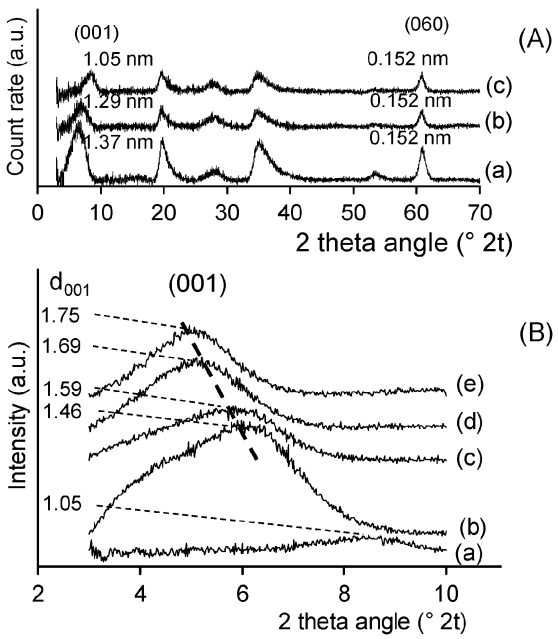

Fig. 8 XRD patterns (A) of (a) RL, (b) 473 K-DL, (c) SDL samples and (B) of (a) SDL, (b) SDL/B-2, (c) SDL/B-4, (d) SDL/B-6 and (e) SDL/B-8 samples with the corresponding inter-reticular distances in nm.

introduction of Brij58 molecules has promoted the stacking of the elementary disc crystals followed by an aggregation to form primary laponite particles. XRD analyses confirmed that the formation of primary laponite particles is aided by surfactant molecules which cover elementary discs so explaining their presence in the interlayer space. At 2 and 4 g L^{-1} Brij58 initial concentrations, the $d_{(001)}$ observed for resulting composites are broader and multicomponent compared to those observed for composites obtained at 6 and 8 g L^{-1} initial concentrations. This indicates a heterogeneous layer stacking distribution probably as a result of a lower degree of organisation for low amount of surfactant.

The porosity of spray-dried laponite and Brij58/laponite samples has been investigated by nitrogen sorption analyses. N_2-adsorption/desorption isotherms and corresponding pore size distributions are reported in Fig. 11A. Calculated data such as surface area (S_{BET}), microporous area (S_{micro}), pore diameter (ϕ_p) and pore volume (V_p) are listed in Table 1. It is worth noting that clay surface areas measured by nitrogen sorption are underestimated.[54]

Isotherms of the surfactant-free materials are type IV_b and exhibit a wide triangular H_2 hysteresis at medium relative pressures. This type of isotherm is characteristic of mesoporous materials. The H_2 hysteresis is both characteristic of ink-bottle-like pores (internal porosity) and small sphere-like particles with interparticular textural porosity. This latter case would correspond to raw and dried laponite samples which, as observed by SEM, are constituted of 30-nm spherical particles. Mesoporosity within the spray-dried laponite sample is also textural but in that case created by aggregation of the large stacked layers that constitute the spherical particles observed for this sample by SEM and TEM. For all samples, the same narrow pore size distribution was observed with an average pore diameter at 4 nm. The BET surface area of raw laponite is quite high (351 m^2 g^{-1}) compared to other clays because the primary particles are very small (25 nm). Although, the BET surface area was in the same value range (Table 1), the contribution of microporosity was much lower for spray-dried laponite sample. This is probably due to the edge-to-edge stacking of stacked elementary disc particles upon the spray-drying process that reduce the textural microporosity observed when stacked elementary discs aggregate, as observed for raw and 200 °C-dried laponite samples. The resulting larger laponite particles create mesoporosity when they aggregate to form the spheres. As a consequence, mesoporosity and pore volume are more important for the spray-dried materials. The N_2 sorption isotherm of this material exhibits also a high increase of N_2 adsorbed volume at high relative pressure (P/P_0 ~0.9) which characterize the presence of large mesopores and macropores. This extra textural porosity can be correlated to the porosity between spheres and the roughness on their surface which may create large mesopores.

Nitrogen adsorption–desorption isotherms of sprayed Brij-laponite composites are illustrated in Fig. 9B and their porous characteristics are listed in Table 1.

Isotherm shapes of SDL/B-2 and SDL/B-4 materials are similar to those of the SDL material, but the total adsorbed volume is lower. Hysteresis loops expand almost in the same

Table 1 N_2-sorption data of RL, SDL and SDL/B-*x* samples: surface area (S_{BET}), microporous area (S_{micro}), pore diameter (σ_p) and pore volume (V_p)

Sample	$S_{BET}/m^2\ g^{-1}$	$S_{micro}/m^2\ g^{-1}$	$\sigma_p{}^a$/nm	$V_p/cm^3\ g^{-1}$
RL	351	166	3–5	0.24
473 K-D laponite	318	137	3–5	0.16
SDL	331	58	3–5	0.29
SDL/B-2	169	147	3–5	0.18
SDL/B-4	89	67	3–5	0.12
SDL/B-6	11	0	n.d.[a]	0.07

[a] Desorption branch. [b] n.d.: there is no signification to determine value in this case.

relative pressures range, indicating that pore sizes and their size distributions are similar. The SDL/B-6 sample presents a type III isotherm and no porosity could be detected for the SDL/B-8 sample. Porous characteristics presented in Table 1 show clearly the decrease of porosity with initial Brij58 concentration. This can be explained by the blocking of the textural porosity within spheres by Brij58 surfactant molecules.

Prior to thermal analyses, all samples were previously dehydrated by oven-drying (303 K) and then re-hydrated under controlled moisture (55%, under saturated $Ca(NO_3)_2$ atmosphere). Thermogravimetric curves are reported in Fig. SM1 of ESI.† The thermograms of surfactant-free samples present a first loss of weight in the 50–200 °C range which is associated to an endothermic phenomenon and corresponds to

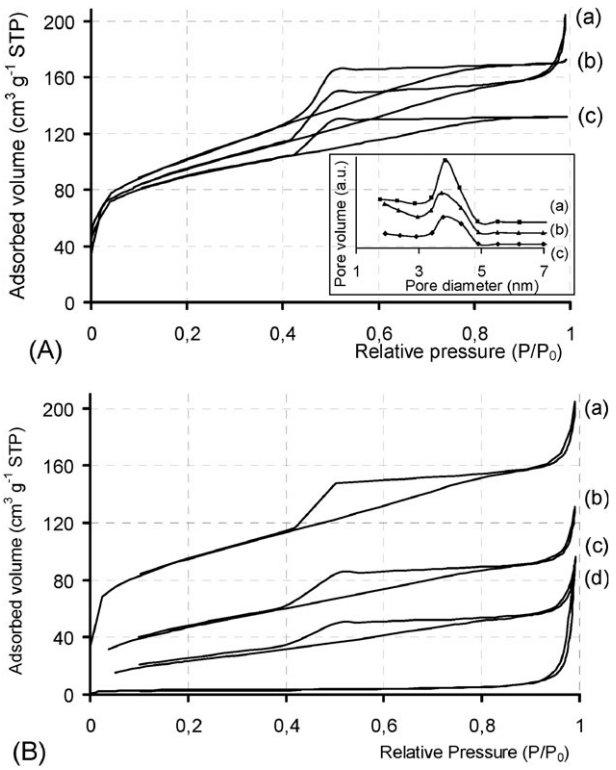

Fig. 9 N_2 adsorption–desorption isotherms and corresponding Halsey modified BJH pore size distributions (A) of (a) SDL, (b) 473 K-DL, (c) RL, and (B) of (a) SDL, (b) SDL/B-2, (c) SDL/B-4 and (d) SDL/B-6 samples

the departure of physisorbed water. The second small weight loss (about 3–4%) in the 200–650 °C range corresponds to the dehydroxylation of Si–OH, Mg–OH and/or Li–OH groups. A third and last weight loss is observed in the 650–750 °C temperature range which is associated to an exothermic phenomenon and corresponds, as confirmed by XRD, to the phase transition from laponite to enstatite. The departure of physisorbed water and the phase transition are also observed in the thermograms of spray-dried Brij58/laponite materials. There is also a weight loss in the 200–650 °C temperature range which is more significant than that observed for surfactant-free laponite samples. This weight loss corresponds mainly to the decomposition of the Brij58 surfactant and less to dehydroxylation. Percentages of weight losses (calculated from curves), the temperatures corresponding to the maxima of the endothermic peaks associated to the departure of water physisorbed (T_w), of the exothermic peaks associated to the surfactant decomposition (T_{Brij}) and of the exothermic peak associated to the phase transition (T_{crist}), the theorical ($\%_{th}$) and experimental ($\%_{exp}$) Brij58 amounts (weight percentages) are reported in Table 2. The weight loss due to physisorbed water is lower for spray-dried Brij58/laponite composites compared to surfactant-free samples. Moreover, this weight loss decreases with an increased amount of adsorbed surfactant molecules. These observations can be related to the adsorption of Brij58 surfactant molecules on the laponite platelet surface that reduce the amount of adsorbed water. It is noteworthy that the endotherms are at lower temperature for Brij58/laponite composites which could be related to the presence of water molecules weakly adsorbed possibly due to the presence of surfactant molecules adsorbed and/or the hydrophobic part of the surfactant molecules. The second weight loss is in quite good agreement with the initial amount of surfactant introduced in the suspension. This weight loss starts at higher temperatures (maxima at 315 °C) for SDL/B-2 and SDL/B-4 samples compared to the reference system Brij58/Quartz (maximum at 247 °C) which could be explained by the interaction between surfactant and the laponite platelet surface. Concerning the two samples SDL/B-6 and SDL/B-8, the presence of two exotherms indicates a mixture of Brij58 surfactant molecules in interaction with the laponite platelet surface (maxima at 315 and 300 °C, respectively) and free Brij58 surfactant molecules (maxima at 245 and 215 °C, respectively). These free surfactant molecules are probably aggregated to those interacting with the clay surface. Concerning the exotherm associated to the phase transition, maxima of temperatures are displaced to higher temperatures for spray-dried samples (*ca.* 750 *cf.* 725 °C). This can be due to the disordered stacking of clay layers (partial delamination) as observed by TEM.

FTIR spectra of surfactant-free materials were found to be similar (Fig. SM2, ESI†): a broad multicomponent band was observed at around 3700–3000 cm^{-1}, in a range of frequencies usually assigned to surface hydroxyl groups and adsorbed water. The main component of this band consists of the overlapping of two components: Si–OH (at 3630 cm^{-1}) and Mg–OH (at 3685 cm^{-1}) stretching vibrations and the ν(O–H) stretching frequency at 3465 cm^{-1} due to physisorbed water.[55] The δ(O–H) deformation band at 1640 cm^{-1} is another

Table 2 Thermal analysis data: percentage weight losses Δw_{50-200}, $\Delta w_{200-650}$ and $\Delta w_{650-750}$ in the 50–200, 200–650 and 650–750 °C temperature ranges (calculated from curves), temperatures corresponding to the maxima of the endothermic peaks associated to the departure of physisorbed water (T_w), of the exothermic peaks associated with surfactant decomposition (T_{Brij}) and of the exothermic peak associated to the phase transition (T_{cryst}), and the theorical ($\%_{th}$) and experimental ($\%_{exp}$) percentages of Brij58

Sample	Δw_{50-200} [T_w/°C]	$\Delta w_{200-650}$ [T_{Brij}/°C]	$\Delta w_{650-750}$ [T_{Cryst}/°C]	$\%_{th}$	$\%_{exp}$
RL	14.2 [130]	3.0	2.1 [727]	—	—
200 °C-L	12.2 [123]	4.5	5.5 [720]	—	—
SDL	16.7 [107]	3.8	2.1 [746]	—	—
SDL/B-2	9.1 [74]	11.3 [**315**; *360*; *380*][a]	1.4 [750]	9.1	12.4
SDL/B-4	5.4 [70]	16.4 [*280*; **315**; 400; **450**][a]	2.3 [750]	16.7	17.3
SDL/B-6	6.6 [67]	24.7 [**245**; ***280***; **315**; *370*][a]	2.0 [750]	27.1	25.8
SP/B-8	3.7 [65]	29.8 [**215**; **300**; *420*][a]	3.7 [745]	28.6	30.9
Brij58/Quartz	0.7 [50]	37.2 [**247**; 360; 430; *460*][a]	—	40.0	37.5

[a] The temperatures corresponding to the main weight losses are shown in bold and the temperatures corresponding to weak endothermic signals (shoulders) are indicated in italics.

indication of the presence of water. In the low energy region, the spectra show one broad band with a maximum peak at 1005 cm^{-1} assigned to Si–O and Si–O–Si stretching vibrations, one band around 660 cm^{-1} due to O–H bending vibration from adsorbed water, and one band at 540 cm^{-1} assigned to Mg–O vibration. Bands characteristic of the clay were also observed in the FTIR spectra of Brij58/laponite nanocomposites (Fig. SM2, ESI†). In addition, these spectra exhibited bands at 2800–3000 cm^{-1} assigned to C–H stretching, and at 1470, 1360, 1345, 1280 and 1245 cm^{-1} assigned to CH deformations, which are relevant to the presence of Brij58 surfactant molecules. It is also interesting to note that the bands observed in the SiO–H and HO–H region (3200–3700 cm^{-1}) and at 1640 cm^{-1} are somewhat less intense indicating a lower amount of adsorbed water, which could be related to a higher hydrophobic character due to the presence of surfactant molecules. As a consequence the sharp bands at 3710 and 3690 cm^{-1} assigned to isolated OH groups from Si–OH and Mg–OH, respectively, are increased in intensity.

Finally, solid-state multinuclear magnetic resonance experiments were performed. The ^{29}Si MAS NMR spectra of raw laponite and spray-dried laponite are presented in Fig. SM3 (ESI†). Two main resonances at −94.8 and −85.1 ppm are clearly observed which correspond to Q^3 and Q^2 units, respectively.[56] Q^3 and Q^2 units represent $(SiO)_3Si–(OMg)$ and $(SiO)_2(MgO)Si–OH$ species, respectively. Q^2 units account for silicon located on the edge of laponite particles. However, the spectral simulation of the spectra with WINFIT software[57] have revealed the presence of two resonances at −94.4 and −97.1 ppm which could be assigned to hydrated and dehydrated $(SiO)_3Si–OMg$ species, respectively. Indeed, Mandair *et al.* have observed a shielding of silicon resonances when laponite was heated at 200 °C.[56] This was attributed to the loss the interlayer water which interacts *via* hydrogen bonding with the basal oxygen atom. Similarly, the signal at −85.1 ppm was simulated with two components at −84.1 and −85.8 ppm, which were assigned to hydrated and dehydrated Q^2 $(SiO)_2(MgO)Si–OH$ species, respectively. Relative amounts of the different Q^2 and Q^3 species were calculated from spectral simulation. The molar ratio Q^2/Q^3, taking into account the low resolution of ^{29}Si MAS NMR techniques is roughly the same for both RL (8.8/91.2) and SDL (7.7/92.3) samples. Therefore, as observed by FTIR, silanol groups do not seem to be affected by the flash drying process.

Due to the presence of surfactant molecules in spray-dried Brij58/laponite materials, ^1H MAS NMR spectra were only recorded on dehydrated raw and spray-dried laponite and are reported in Fig. SM4 (ESI†). Three resonances with similar intensity and broadness were distinguished from ^1H NMR spectra recorded on surfactant-free materials. The most intense signal at 0.4 ppm, can be assigned to MgOH located in the octahedral layers of laponite platelets.[58] The shoulder observed at −0.6 ppm was assigned, in agreement with the literature, to hydrogen-bond donor OH groups linked to Mg nuclei.[59] Finally, the small resonance observed at 1.6 ppm may be assigned to Si–OH groups of the tetrahedral layers.[60]

From ^{29}Si and ^1H NMR data it seems that no change has occurred at the hydroxyl group level indicating no condensation under spray-drying.

For both raw and sprayed laponite samples, one ^7Li MAS NMR resonance was observed at −0,4 ppm (spectra not shown). As the chemical shift and intensity of the signal are similar for both samples, it can be concluded that the spray-drying process did not affect the local environment of lithium atoms in the materials.

The ^{13}C CP-MAS solid-state NMR spectra of Brij58/laponite nanocomposites are presented in Fig. 10. Resonance lines were assigned according to a liquid ^{13}C NMR simulated spectrum with ACD/I-LAB software.[61,62] Spectra show resonances in the 12–38 ppm region, which are attributed to CH_2 and CH_3 groups of the alkyl chain, and resonances in the 48–75 ppm region, which are attributed to CH_2 groups of the polyethylene oxide chain. ^{13}C NMR data confirm the presence of Brij58 molecules as observed by FTIR and confirm their integrity. Variation in the chemical shifts, intensities and resolution of CH_3 and CH_2 lines from both alkyl and polyethylene oxide chains are most probably due to change of conformation of chains and different chain-to-chain interactions as a consequence of the aggregation type with increased surfactant amount on the clay surfaces.

FTIR did not show any relevant change in bands characteristic of silanol groups. However, TEM showed that stacked layers particles have associated edge-to-edge to each other to form ~100 nm-length clay layers. Moreover, the fact that spray-dried spherical laponite particles are stable in water is indicative of the strong interaction of stacked primary laponite particles

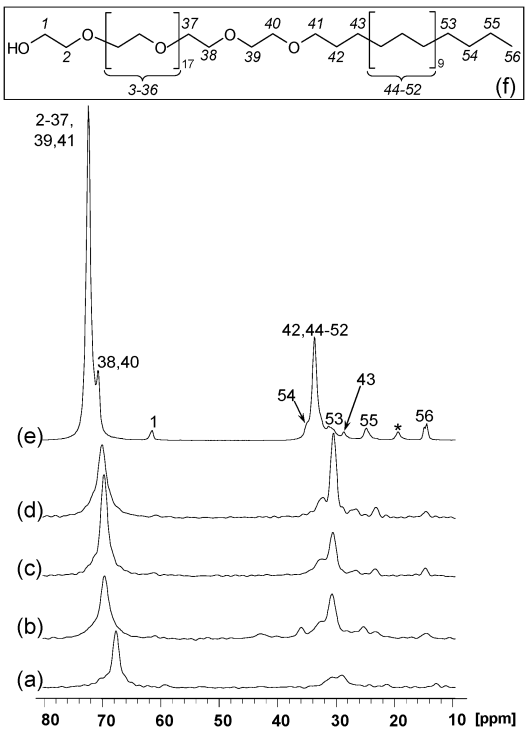

Fig. 10 ^{13}C NMR spectra of sprayed Brij58/laponite composites: (a) SDL/B-2, (b) SDL/B-4, (c) SDL/B-6, (d) SDL/B-8 and (e) pure Brij58. The formula and carbon assignation of Brij58 are shown in inset (f).

and aggregates. NMR and FTIR techniques are probably not sensitive enough to detect Si–O–Si bridge formation during the spray-drying process. Quantitative ^{1}H NMR experiments could help to detect the condensation of a few Si–OH groups.

Mechanism of formation

As is usually observed, laponite particles were initially delaminated in water. DLS is consistent with the main presence of isolated and/or stacked layers. It is noteworthy that the concentration 20 g L^{-1} is above the gelation concentration for laponite (C_g = 9 g L^{-1}) and corresponds to the limit of birefringence area (C_{NI}).[63] Above this concentration, laponite platelets form liquid crystal mesophases. Nevertheless, DLS has indicated a size distribution ranging from 5 to 30 nm for 24 h-aged (under stirring) 1, 5 and 20 g L^{-1} salt-free laponite suspensions in distilled water (although this technique is not really adapted to determine hydrodynamic radii of thin disc particles such as laponite elementary crystal discs). However, a size distribution from 40 to 80 nm was observed for a 7-day-aged (24 h under stirring and 6 days under static conditions) 20 g L^{-1} salt-free laponite suspension. 24 h-aged (under stirring) suspensions are probably composed of isolated and stacked elementary laponite crystal discs while aggregates were formed in the 7-day-aged sample. When Brij58 surfactant molecules are introduced in the medium, these layers are covered by surfactant molecules and stacked *via* surfactant/surfactant interactions. After spray-drying, micron-size spherical particles are formed from both laponite and Brij58/laponite suspensions. The laponite structure was revealed by XRD indicating that the 473 K flash-drying induces a stacking of the layers by self-assembling in a closed volume delimited by the droplet size. Moreover, TEM revealed the edge-to-edge stacking of the stacked particle layers resulting in the formation of 100 nm-length and 30 nm-height layered particles that agglomerate with each other within water droplets to form spherical particles. Interlayer distances d_{001} were higher for Brij58/laponite composites and increased with increased surfactant loading as a consequence of the presence of the surfactant molecules in the interlayer space. Stacking of layers was found to be less ordered by XRD for spray-dried materials. This is probably a consequence of the fast drying process. As it was showed by Gabriel *et al.*,[63] laponite nanolayers form liquid crystalline (LC) mesophases at high concentration, whose structures depend on the clay concentration. This means that in our system, several LC mesophases probably occurred and succeeded each other during the drying process until one freeze. *In situ* SAXS measurements would help to follow the phase transitions, evaluate the transition kinetics and identify the different mesophases.[64]

Partial delamination was also observed for spray-dried Brij58/laponite composite particles with the delamination degree increasing with the amount of surfactant loading. This

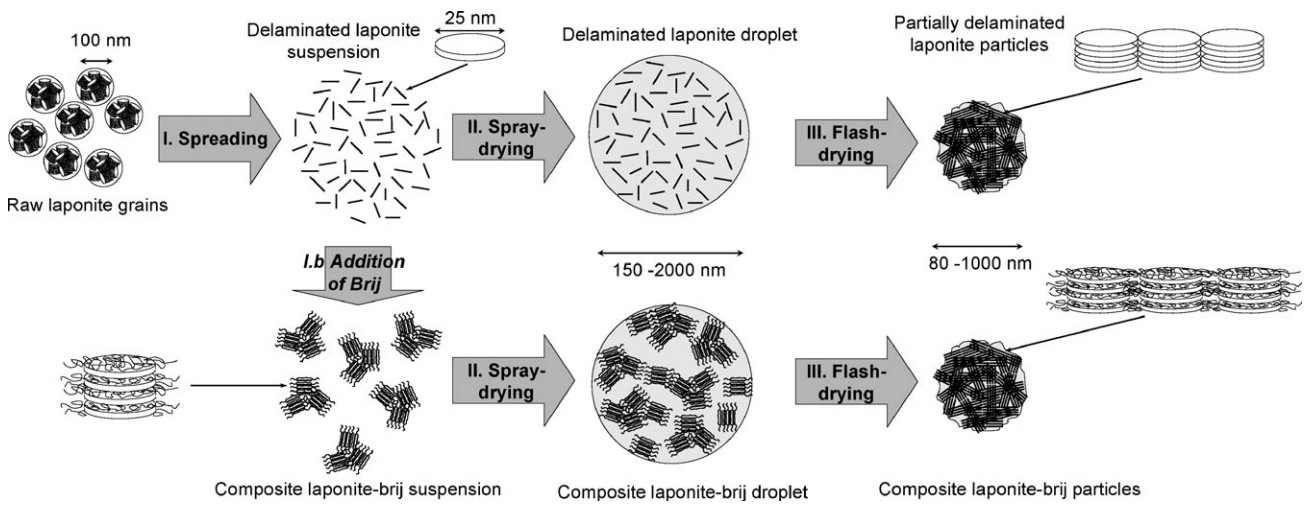

Fig. 11 Schematic representation of the proposed mechanism of formation.

is related to the presence of surfactant molecules in the interlayer space. As observed by SEM and TEM, a spherical particle formed under spray-drying presents a significant surface roughness due to the aggregation of plate-like particles within the water droplets. As a consequence, textural mesoporosity was created inside and between the spheres and the microporosity was decreased (N_2-sorption analyses). The proposed mechanism of formation is schematically represented in Fig. 11. Finally, spray-dried laponite particles are stable over several days when they are spread into distilled water, unlike raw laponite particles, indicating that stacked laponite elementary discs are strongly linked together. However, no condensation between SiOH edge groups was observed by either NMR and FTIR.

Conclusion

An aerosol process that combines both the use of nanobuilding blocks and the confinement of reaction volume inside droplets has been used to form laponite and Brij58/laponite nanocomposite spherical micron-size particles. Several techniques have been used to characterize and get better insight in the formation mechanism of these macrostructures. Quasi-spherical clay particles were obtained by a spray-drying treatment on a laponite colloidal suspension in the presence or absence of Brij58 surfactant. Sphere sizes ranged from 70 to 1000 nm with an average size of about 220 nm. Laponite elementary crystal discs used as nanobuilding blocks stack face-to-face and edge-to-edge to form layered particles with clay structure, which aggregate in larger spherical particles. Adding Brij58 to the initial laponite suspension allows not only to slow down the gelification process by steric protection of the laponite discs, but also links elementary disc crystals. As a consequence, the interlayer space is larger in spray-dried Brij58/laponite composites than in spray-dried laponite. All spherical particles prepared by spray-drying were found to be partially delaminated. A mechanism has been proposed to explain the formation of these particles: a re-stacking of delaminated layers that occurs under the fast drying of the laponite suspension associated with the aerosol process.

Unlike raw laponite, spray-dried laponite-based materials are stable in water. This stability is very interesting for applications such as sorbents for contaminants in liquid media. Indeed, macrostructures can be easily separated from the solution and reduce charge effects if used in filtering devices. These macrostructures present a high surface area such as laponite nanoparticles but with a larger mesoporosity proportion. The presence of mesoporosity inside spheres allows diffusion of large molecules and may help in species diffusion. Moreover, the laponite structure confers ionic exchange ability. Concerning the Brij58/laponite composites, the presence of surfactant molecules renders the composite more hydrophobic and enhances its sorption properties for organic molecules.

Experimental

Materials

All chemicals were used as received. Raw laponite (RD grade) was provided by Rockwood Additives Ltd with the following

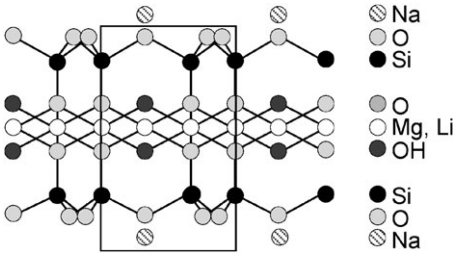

Fig. 12 Schematic representation of the laponite™ unit cell (inspired from ref 39)

chemical formula: $Na_{0.7}{}^{+}((Si_8Mg_{5.5}Li_{0.3})O_{20}(OH)_4)^{-0.7}$.[39] This trioctahedral phyllosilicate is composed of tetrahedral layers filled by Si atoms linked by oxygens and octahedral layers are constituted of Mg and Li atoms linked by oxygens and hydroxyl groups. This substitution creates a deficit in the positive charges which is balanced by sodium cations located in the interlayer space. As shown in Fig. 12, the laponite unit cell size is $0.53 \times 0.92 \times 1$ nm.[65]

The non-ionic surfactant Brij58 was purchased from Fluka. This amphiphilic diblock copolymer is an poly(ethyleneoxide)-alkyl ether surfactant of formula is $C_{16}H_{33}(OC_2H_4)_{20}OH$.

Preparation of the laponite and Brij58/laponite suspensions

In a typical preparation, laponite suspension is prepared by spreading raw laponite powder into 500 mL of distilled water at a 20 g L^{-1} concentration under stirring at room temperature. The resulting suspension is then maintained under stirring for 24 h before the spray-drying process. For Brij58-laponite systems, the solid Brij58 surfactant is added to the homogeneous laponite suspension (before aging under stirring for 24 h) to a concentration ranging from 2 to 8 g L^{-1}.

Spray-drying treatment

The spray drying apparatus is composed of a constant output atomizer (TSI model 3076), nominally providing droplet particles of 2000 nm mean diameter, at a fixed N_2 gas pressure of 2 bar. The solution was pumped-out and sprayed-out of the atomizer in the form of fine particles that were then carried by the N_2 gas flux to a tubular furnace operating at 473 K allowing the evaporation of water. Dried particles were collected on a 200 nm membrane filter. The spray-drying set-up is also composed with a vacuum flask refrigerated with an ice-bath to condense water and a vacuum pump to keep the

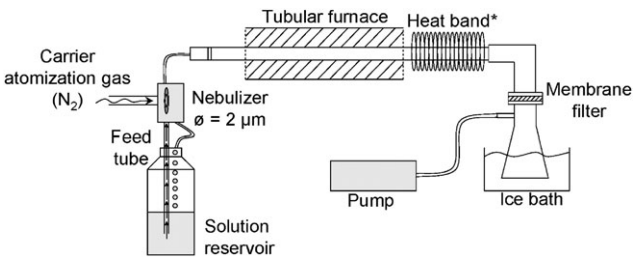

Fig. 13 General scheme of the spray-drying apparatus. *The heat band allows to maintain an elevated temperature to avoid water condensation in the glass tube.

Table 3 Experimental conditions for NMR acquisitions

Nucleus	Probe head	Resonance frequency, ω_0/MHz	Technique	Pulse width/μs	Angle/rad	Repetition delay/s	Contact time/ms	No. of scans
^{29}Si	7 mm	59,63	MAS-DEC[a]	1.33	π/6	80	—	~600
^{13}C	7 mm	75,48	CP[b]-MAS	4.7	π/2	4	2	>14000
^{1}H[c]	2.5 mm	300,14	MAS	3.03	π/2	2	—	600
^{7}Li	2.5 mm	116,64	MAS	1.03	π/8	0.4	—	3750

[a] DEC = proton decoupling. [b] CP = ^{1}H–^{13}C crossed polarization. [c] ^{1}H NMR spectroscopy analyses, samples have been previously dehydrated for 24 h at 363 K under vacuum to remove adsorbed water.

gas flux constant in a laminar regime. A global scheme is shown in Fig. 13.

As a reference sample, a part of the laponite suspension was dried at 473 K in an oven overnight (sample 473 K-DL).

Characterization techniques

Apparent densities were determined from the mass and the global volume occupied by the dried samples placed in a cylindrical vial. An average value was determined from volume measurements taken just after filling the vial with the clay sample and after packing down the powder by gently tapping the filled vial on the bench.

Dynamic light scattering (DLS) measurements were performed using a Malvern Instruments ZetaSiser NanoZS equipped with a He–Ne laser (λ = 633 nm). Particle sizes were calculated using a non-negative-least-square (NNLS) algorithm. Measurements, repeated five times for each sample, were made on as-made initial suspensions and spray-dried powder spread out in distilled water at a ~5 g L^{-1} concentration.

X-Ray diffraction (XRD) patterns were recorded on a Philips X'Pert diffractometer (Cu-Kα radiation: λ = 0.15406 nm, 2θ scan range: 3–70°, step size: 0.02°/2s) equipped with a X'celerator detector.

Simultaneous thermogravimetric and differential thermal analyses (TGA/DTA) were carried out in simulated dry air (O_2/N_2 mixture) on a Setaram Labsys thermoanalyser. The temperature profile ranged from 298 to 1073 K with a heating rate of 5 K min^{-1}, using alumina as a reference.

Nitrogen sorption analyses were obtained with a Micromeritics Tristar sorptometer using standard continuous procedures at 77.15 K on samples that had been degassed at 363 K for 1 h and then at 403 K under high vacuum for at least 10 h. Surface area was calculated according to the Brunauer–Emmett–Teller (BET) model[66] over a relative pressure range of 0.05–0.30; microporous area was calculated according to the t-plot method. Pore diameter distribution was calculated according to the Barret–Joyner–Halenda (BJH) method,[67] modified by the Halsey thickness curve correction[68] on the desorption branch.

Scanning electron microscopy (SEM) was carried out on a Philips XL 30 microscope equipped with a field-emission gun (FEG) operating at 7 kV accelerating voltage. The samples were previously deposited on carbon tape and sputter-gold-coated.

Transmission electron microscopy (TEM) was performed on a Philips CM 200 microscope operating at 200 kV (LaB_6 filament). As-prepared colloidal suspensions or solid samples spread out in distilled water at ~1 g L^{-1} were deposited onto carbon and formvar-coated 200 mesh copper grids.

Fourier-transform infrared (FTIR) spectroscopy was run in the transmission mode with a Bruker equinox 55 FRA 106/S spectrometer operating over a range from 400 to 5000 cm^{-1}, with a 2 cm^{-1} resolution (32 scans). 1 cm-diameter pellets were prepared by mixing 1 mg of the sample to analyze with 100 mg of dried KBr.

Magic angle spinning (MAS) multinuclear (^{1}H, ^{7}Li, ^{13}C and ^{29}Si) magnetic resonance (NMR) experiments were run on a Brucker Avance 300 spectrometer (B_0 = 7.1 T) using conditions reported in Table 3.

Acknowledgements

We would like to thank Dr S. Rigolet and Pr C. Marichal for their assistance and comments concerning NMR spectroscopy. Rockwood Ltd is also acknowledged for the gift of laponite RD.

References

1 R. Brayner, *Nano Today*, 2008, **3**(1–2), 48–55.
2 D. Baechi, R. Buser and J. Dual, *J. Nanoparticle Res.*, 2000, **2**, 393–399.
3 H. Zeng, J. Li, J. P. Liu, Z. L. Wang and S. Sun, *Nature*, 2002, **420**, 395–398.
4 Z. Liu, L. Ci, N. Y. J in-Phillipp and M. Rühle, *J. Mater. Chem.*, 2007, **17**, 4619–4625.
5 C. Sanchez, G. J. de A. A. Soler-Illia, F. Ribot, T. Lalot, C. R. Mayer and V. Cabuil, *Chem. Mater.*, 2001, **13**, 3061–3083.
6 H. Bönnemann, W. Brijoux, R. Brinckmann, T. Joußen, B. Korall and E. Dinjus, *Angew. Chem., Int. Ed.*, 1991, **30**, 1312–1314.
7 M. I. Reetz and S. R. Waldrogel, *Angew. Chem., Int. Ed.*, 1997, **36**, 865–867.
8 H. A. Matting and W. Brockmann, *Angew. Chem., Int. Ed.*, 1968, **7**, 598–605.
9 H. W. Ch. Postma, T. Teepen, Z. Yao, M. Grifoni and C. Dekker, *Science*, 2001, **293**, 76–79.
10 Y. Huang, X. F. Duan, Y. Cui, L. J. Lauhon, K. H. Kim and C. M. Lieber, *Science*, 2001, **294**, 1313–1317.
11 T. Rueckes, K. Kim, E. Joselevich, G. Y. Tseng, C. L. Cheung and C. M. Lieber, *Science*, 2000, **289**, 94–97.
12 Y.-W. Jun, J.-W. Seo, S. J. Oh and J. Cheon, *Coord. Chem. Rev.*, 2005, **249**, 1766–1775.
13 R. Jin, Y. Cao, C. A. Mirkin, K. L. Kelly, G. C. Schatz and J. G. Zheng, *Science*, 2001, **294**, 1901–1903.
14 J. S. Bradley, B. Teschte, W. Busser, M. Maase and M. T. Reetz, *J. Am. Chem. Soc.*, 2000, **122**, 4631–4636.
15 V. F. Puntes, D. Zanchet, C. K. Erdonmez and A. P. Alivisatos, *J. Am. Chem. Soc.*, 2002, **124**, 12874–12880.
16 S.-M. Lee, Y.-W. Sun, S.-N. Cho and J. Cheon, *J. Am. Chem. Soc.*, 2002, **124**, 11244–11245.

17 S. Diré, G. Brusatin, M. L. Di Vona, P. Egger, M. Ferrari, P. Innocenzi, S. Licoccia, P. Romagnoli, M. Trombetta and L. Zampedri, *J. Eur. Ceram. Soc.*, 2005, **25**, 2051–2054.
18 P. Fratzl, *Curr. Opin. Colloid Interface Sci.*, 2003, **8**, 32–39.
19 M. Stark, S. Grip, A. Rising, M. Hedhammar, W. Engstroem, G. Hjaelm and J. Johansson, *Biomacromolecules*, 2007, **8**, 1695–1701.
20 H. Wang, C. Xie, D. Zeng and Z. Yang, *J. Colloid Interface Sci.*, 2006, **297**, 570–577.
21 S. Ding, J. Guo, X. Yan, T. Lin and K. Xuan, *J. Cryst. Growth*, 2005, **284**, 142–148.
22 M. Mo, J. C. Yu, L. Zhang and S.-K. Li, *Adv. Mater.*, 2005, **17**, 756–760.
23 L. Huerta, C. Guillem, J. Latorre, A. Beltran, D. Beltran and P. Amoros, *Solid State Sci.*, 2005, **7**, 405–414.
24 S.-B. Xiang and X. Xiang, *Mater. Lett.*, 2007, **61**, 3662–3665.
25 H. Yi, H. Song and X. Chen, *Langmuir*, 2007, **23**, 3199–3204.
26 P. Yang, T. Deng, D. Zhao, P. Feng, D. Pine, B. F. Chmelka, G. M. Whitesides and D. Stucky, *Science*, 1998, **282**(5397), 2244–2246.
27 K. Master, in *Spray-Drying Handbook*, ed. Longman Scientific and Technical, Harlow, 1990.
28 Y. Lu, H. Fan, A. Stump, T. L. Ward, T. Riecker and C. J. Brinker, *Nature*, 1999, **398**, 223–226.
29 C. J. Brinker, Y. Lu, A. Sellinger and H. Fan, *Adv. Mater.*, 1999, **11**, 579–585.
30 G. V. Rama Rao, G. P. Lopèz, J. Bravo, H. Pham, A. K. Datye, H. Xu and T. L. Ward, *Adv. Mater.*, 2002, **14**, 1301–1304.
31 M. T. Bore, S. B. Rathod, T. L. Ward and A. K. Datye, *Langmuir*, 2003, **19**, 256–264.
32 N. Baccile, D. Grosso and C. Sanchez, *J. Mater. Chem.*, 2003, **13**, 3011–3016.
33 I. V. Melnyk, Y. L. Zub, E. Véron, D. Massiot, T. Cacciaguerra and B. Alonso, *J. Mater. Chem.*, 2008, **18**, 1368–1382.
34 P. J. Bruinsma, A. Y. Kim, J. Liu and S. Baskaran, *Chem. Mater.*, 1997, **9**, 2507–2512.
35 D. Grosso, G. J. A. A. Soler-Illia, E. L. Crepaldi, B. Charleux and C. Sanchez, *Adv. Funct. Mater.*, 2003, **13**, 37–42.
36 M. Jaber, F. O. M. Gaslain and J. Miehé-Bredlé, *Clays Clay Miner.*, in press.
37 F. Iskandar, Mikrajuddin and K. Okuyama, *Nano Lett.*, 2001, **1**, 231–234.
38 Laponite technical data sheet, www.Laponite.com, Rockwood Additives Limited.
39 L. M. Daniel, R. L. Frost and H. Y. Zhu, *J. Colloid Interface Sci.*, 2007, **316**, 72–79.
40 J. M. Saunders, J. W. Goodwin, R. M. Richardson and B. Vincent, *J. Phys. Chem. B*, 1999, **103**, 9211–9218.
41 Z. Grauer, D. Avnir and S. Yariv, *Can. J. Chem.*, 1984, **62**, 1889–1894.
42 S. Yariv, M. Muller-Vonmoos, G. Kahr and A. Rub, *J. Therm. Anal. Calorim.*, 1989, **35**, 1941–1952.
43 B. Brahimi, P. Labbe and G. Reverdy, *Langmuir*, 1992, **8**, 1908–1918.
44 A. de M. F. Guimaraes, V. S. T. Ciminelli and W. L. Vasconcelos, *Mater. Res.*, 2007, **10**, 37–41.
45 P. Mongondry, T. Nicolai and J.-F. Tassin, *J. Colloid Interface Sci.*, 2004, **275**, 191–196.
46 Several Brij surfactants Brij 56, Brij 58, Brij 97, Brij 700. were tested under our conditions (laponite water suspension at 20 g L^{-1} and surfactant at 2–8 g L^{-1}) and only Brij 58 surfactant gave stable colloidalsuspensions without gelling.
47 T. Nicolaï and S. Cocard, *Langmuir*, 2000, **16**, 8189–8293.
48 J. D. F. Ramsay and P. Lindner, *J. Chem. Soc., Faraday Trans.*, 1993, **89**, 4207–4214.
49 A. Mourchid, A. Delville, J. Lambard, E. Lécolier and P. Levitz, *Langmuir*, 1995, **11**, 1942–195048; Y. Qi, M. Al-Mukhtar, J.-F. Alcover and F. Bergaya, *Appl. Clay Sci.*, 1996, **11**, 185–197.
50 F. Pignon, A. Magnin, J.-M. Piau, B. Cabane, P. Lindner and O. Diat, *Phys. Rev. E*, 1997, **56**, 3281–3289.
51 A. Nelson and T. Cosgrove, *Langmuir*, 2004, **20**, 2298–2304.
52 A. Nelson and T. Cosgrove, *Langmuir*, 2004, **20**, 10382–10388.
53 J. M. Fraile, J. I. Garcia, J. Massam and J. A. Mayoral, *J. Mol. Catal., A*, 1998, **136**, 47–57.
54 V. Médout-Marère, H. Belarbi, P. Thomas, F. Morato, J. C. Giuntini and J. M. Douillard, *J. Colloid Interface Sci.*, 1998, **202**, 139–148.
55 M. D'Angelo, A. Fuccello, G. Onori and A. Santucci, *Prog. Colloid Polym. Sci.*, 1993, **83**, 350.
56 A.-P. S. Mandair, P. J. Michael and W. R. MacWhinnie, *Polyhedron*, 1990, **9**, 517–525.
57 D. Massiot, F. Fayon, M. Capron, I. King, S. Le Calvé, B. Alonso, J.-O. Durand, B. Bujoli, Z. Gan and G. Hoatson, *Magn. Reson. Chem.*, 2002, **40**, 70–76.
58 S. Borsacchi, M. Geppi, L. Ricci, G. Ruggeri and C. A. Veracini, *Langmuir*, 2007, **23**, 3953.
59 C. Chizallet, G. Costentin, H. Lauron-Pernot, M. Che, C. Bonhomme, J. Maquet, F. Delbecq and P. Sautet, *J. Phys. Chem. B*, 2007, **111**, 18279–18287.
60 G. Hartmeyer, C. Marichal, B. Lebeau, S. Rigolet, P. Caullet and J. Hernandez, *J. Phys. Chem. C*, 2007, **111**, 9066–9071.
61 A. J. Williams, *ChemNewsCom*, 1999, **9.4**, 16–18.
62 Advanced Chemistry Development/Interactive Lab, http://ilab.acdlabs.com.
63 J.-C. P. Gabriel, C. Sanchez and P. Davidson, *J. Phys. Chem.*, 1996, **100**, 11139–11143.
64 C. Boissière, D. Grosso, H. Amenitsch, A. Gibaud, A. Coupé, N. Baccile and C. Sanchez, *Chem. Commun.*, 2003, 2798–2799.
65 Y. Qi, M. Al-Mukhtar, J.-F. Alcover and F. Bergaya, *Appl. Clay Soc.*, 1996, **11**, 185–197.
66 S. Brunauer, P. H. Emett and E. Teller, *J. Am. Chem. Soc.*, 1938, **60**, 309–319.
67 E. P. Barrett, L. G. Joyner and P. P. Halenda, *J. Am. Chem. Soc.*, 1951, **73**, 373–380.
68 G. D. Halsey Jr., *J. Chem. Phys.*, 1948, **16**, 931–937.

